Numerical Solution of the 2D Porous Medium Equation Using Mimetic Difference Operators

Kartiki Pande and Miguel A. Dumett

May 6, 2026

Publication Number: CSRCR2026-07

Computational Science & Engineering Faculty and Students Research Articles

Database Powered by the Computational Science Research Center Computing Group & Visualization Lab

COMPUTATIONAL SCIENCE & ENGINEERING

SAN DIEGO STATE UNIVERSITY

Computational Science Research Center
College of Sciences
5500 Campanile Drive
San Diego, CA 92182-1245
(619) 594-3430

Numerical Solution of the 2D Porous Medium Equation Using Mimetic Difference Operators

Kartiki Pande* Miguel A. Dumett‡

May 6, 2026

Abstract

This work presents a numerical solution of the two-dimensional porous medium equation (PME) using mimetic differences operators provided by the Mimetic Operators Library Enhanced (MOLE) library in MATLAB. The nonlinear diffusion operator $\nabla \cdot (u^m \nabla u)$ is discretized with MOLE's `grad2D` and `div2D` routines, and the semi-discrete system is advanced in time with an implicit Euler scheme. The numerical solution is validated against the analytically known Barenblatt self-similar solution on the domain $[-2, 3] \times [-2, 3]$ from $t_0 = 0.1$ to $t = 0.5$.

*Computational Science PhD Program at San Diego State University / UC Irvinne(`kpande3289@sdsu.edu`).

†Editor: Jose E. Castillo.

‡Computational Science Research Center at San Diego State University (`mdumett@sdsu.edu`).

1 Introduction

Reaction–diffusion equations with nonlinear diffusion arise in a wide range of applications including population dynamics, groundwater flow, and biological pattern formation [1]. Among these, the *porous medium equation* (PME) is a canonical model for density-dependent diffusion in which the effective diffusivity vanishes where the population is absent, giving rise to a compact support that propagates at finite speed.

The objective of this project is to implement a mimetic discretization of the two-dimensional PME using the MOLE library and to validate the numerical solution against the analytically known Barenblatt self-similar solution. The remainder of the report is organized as follows. Section 2 reviews related numerical approaches. Subsection 2.3 states the mathematical problem. Section 3 describes the mimetic discretization and time integration scheme. Section 4 presents the numerical results and error analysis. Section 5, and section 6 summarizes the findings and discusses potential extensions.

2 Background and Related Work

2.1 The Porous Medium Equation

The porous medium equation belongs to the broader family of nonlinear diffusion equations in which the effective diffusivity depends on the solution itself. Its physical origins lie in the study of gas flow through porous rock, where Darcy's law gives rise to a diffusion coefficient proportional to u^{m-1}, so that the flux vanishes wherever the density is zero [4]. Related applications include groundwater infiltration, heat transfer in plasma, and population dynamics, where individuals disperse only into regions they already occupy. In the biological setting considered here, $u(x, y, t)$ represents population density and the exponent $m > 1$ controls how strongly diffusion is suppressed at low densities.

The most important qualitative feature of the PME is the *finite speed of propagation*: unlike linear diffusion, where a compactly supported initial condition instantaneously spreads to the entire domain, the PME solution retains a compact support that expands at a finite rate. This makes the PME physically meaningful for modeling species whose range is genuinely bounded at any finite time. At the edge of the support, $u \approx 0$ and the diffusivity u^{m-1} vanishes, producing a sharp moving front that poses challenges for numerical methods.

The fundamental exact solution of the PME is the *Barenblatt self-similar solution* [4], which plays the same role for the PME as the Gaussian plays for the linear heat equation. Its explicit form is given in Equation (5): the exponents $\beta_t = 1/(m+1)$ and $\beta_r = 1/(2(m+1))$ govern, respectively, the algebraic decay of the peak density and the power-law growth of the support radius over time. For the parameter value $m = 4$ used in this study, $\beta_t = 1/5$ and $\beta_r = 1/10$. As $m \to 1$ the Barenblatt profile approaches a Gaussian, recovering linear diffusion in the limit.

2.2 Classical Finite-Difference Discretizations

The standard finite-difference approach to the PME, as presented in Rostamian [1], approximates the nonlinear diffusion operator $\nabla \cdot (u^m \nabla u)$ with a five-point stencil in which the variable coefficient u^m is evaluated at grid midpoints between adjacent cell centers. After spatial discretization a nonlinear ODE system is obtained, which can be advanced in time with an explicit, semi-implicit, or fully implicit integrator depending on the desired stability properties. This approach is straightforward to implement and works well for smooth solutions on regular grids.

Two principal difficulties arise in practice. First, near the *free boundary* — the moving front where $u \approx 0$ — the diffusivity u^m vanishes and the coefficient matrix becomes nearly singular. Standard stencil truncation in this region can produce negative values or spurious oscillations, requiring explicit positivity corrections such as clipping u to zero after each solve. Second, the diffusion operator introduces *stiffness* that scales like h^{-2} as the grid is refined, imposing a prohibitively small time step $\Delta t \sim h^2 / \max(u^m)$ for explicit schemes. Implicit time integration alleviates this restriction at the cost of solving a nonlinear system at each step.

A further limitation of classical finite-difference stencils is that near-boundary rows are typically derived by ad hoc truncation of interior stencils, which can break discrete conservation properties. In particular, there is no guarantee that the discrete flux across a control volume exactly balances in the way the continuous divergence theorem requires. This motivates the use of mimetic operators, which are constructed from the outset to satisfy such identities.

2.3 Mimetic Differences Method and the MOLE Library

Mimetic differences method aim to preserve, at the discrete level, the fundamental structural identities of the continuous vector calculus operators [2]. Rather than seeking only pointwise truncation accuracy, mimetic operators are constructed so that the discrete gradient $\mathbf{G}$ and divergence $\mathbf{D}$ satisfy an exact discrete analog of Green's first identity under weighted inner products $\langle \cdot, \cdot \rangle_Q$ and $\langle \cdot, \cdot \rangle_P$:

$$h\langle \mathbf{DV},\, F \rangle_Q + h\langle \mathbf{V},\, \mathbf{G}F \rangle_P = \text{boundary terms}, \tag{1}$$

where $\mathbf{V}$ is a face-centered flux vector and F is a cell-centered scalar field. This identity ensures that the discrete flux balance across any control volume is exact, a property that standard finite-difference stencils do not generally satisfy near boundaries where stencil truncation is required. As a consequence, mimetic operators provide a principled and consistent treatment of boundary conditions without the need for ad hoc modifications.

The MOLE library (Mimetic Operators Library Enhanced) [3] provides production-quality implementations of mimetic gradient, divergence, and Laplacian operators as sparse MATLAB matrices. The two-dimensional operators `grad2D` and `div2D` are constructed via Kronecker products of their one-dimensional counterparts, a structure that preserves the separability of the continuous Laplacian and ensures the resulting matrices remain sparse and efficient for implicit linear solves. An interpolation operator `interpol2D` is also provided to

map cell-centered values to face centers, enabling evaluation of the nonlinear coefficient u^m at the locations required by the flux computation.

The operator splitting $\mathbf{D}\cdot\mathbf{K}\cdot\mathbf{G}$, where $\mathbf{K} = \mathrm{diag}(u^m)$ is the nonlinear diffusivity evaluated at face centers, is a natural fit for the PME. Because the governing equation is itself a divergence of a flux, the mimetic div-grad decomposition exactly mirrors the continuous structure of the operator, ensuring discrete flux conservation even at the support boundary where $u^m \to 0$. This structural consistency is the primary motivation for replacing the classical five-point stencil of finite-differences.

We consider the two-dimensional porous medium equation on the domain $\Omega = [-2, 3]\times[-2, 3]$ over the time interval $t \in [t_0, T]$ with $t_0 = 0.1$ and $T = 0.5$:

$$u_t = \alpha \left[\frac{\partial}{\partial x}\left(u^m \frac{\partial u}{\partial x} \right) + \frac{\partial}{\partial y}\left(u^m \frac{\partial u}{\partial y} \right) \right], \qquad (x, y) \in \Omega,\ t > t_0, \tag{2}$$

where $u(x, y, t) \geq 0$ denotes population density, $m > 1$ controls the strength of the nonlinear diffusion, and $\alpha > 0$ is the diffusion coefficient. Parameter values used in this study are $\alpha = 1.0$ and $m = 4$.

2.4 Boundary and Initial Conditions

Homogeneous Dirichlet conditions are imposed on all four walls:

$$u(x, y, t) = 0, \qquad (x, y) \in \partial\Omega,\ t \geq t_0. \tag{3}$$

The solution is initialized with the Barenblatt profile at $t = t_0$:

$$u(x, y, t_0) = \max\big(C - \kappa\, r^2,\ 0\big)^{1/m}, \qquad r^2 = (x - x_c)^2 + (y - y_c)^2, \tag{4}$$

where the center is $(x_c, y_c) = (0.5, 0.5)$, $\kappa = 1/(4\,\alpha\, m\, t_0)$, and $C = 0.5$.

2.5 Exact Barenblatt Solution

The Barenblatt self-similar solution provides an exact reference at any time $t > 0$:

$$u_{\mathrm{exact}}(x, y, t) = \left(\frac{t_0}{t} \right)^{\beta_t} \max\left(C - \kappa\, \frac{r^2}{(t/t_0)^{2\beta_r}},\ 0 \right)^{1/m}, \tag{5}$$

with $\beta_t = 1/(m + 1)$ and $\beta_r = 1/(2(m + 1))$.

3 Numerical Method

3.1 Spatial Discretization with MOLE

The domain Ω is covered by a uniform staggered grid with $n_x = n_y = 160$ interior cells and mesh spacings $\Delta x = \Delta y = 5/160$. Cell-centered unknowns are stored in a vector $\mathbf{U}(t) \in \mathbb{R}^{(n_x+2)(n_y+2)}$ (including two ghost-cell layers per direction).

Spatial derivatives are approximated using three MOLE routines:

- `grad2D`$(k, n_x, \Delta x, n_y, \Delta y)$ — mimetic gradient mapping cell centers to faces;
- `div2D`$(k, n_x, \Delta x, n_y, \Delta y)$ — mimetic divergence mapping faces to cell centers;
- `interpol2D`$(n_x, n_y, 1, 1)$ — interpolation of cell-center values to face centers.

Both operators are constructed with accuracy order $k = 2$.

3.2 Nonlinear Coefficient Assembly

At each time step, face-centred interpolated values $\tilde{u}_f = \texttt{interpol2D} \cdot \mathbf{U}^n$ are used to form the diagonal diffusivity matrix

$$\mathbf{K}(\tilde{u}_f) = \operatorname{diag}\left(\tilde{u}_f^m\right). \tag{6}$$

The discrete nonlinear diffusion operator is then $\mathbf{L}(\mathbf{U}) = \alpha\, \mathbf{D}\, \mathbf{K}\, \mathbf{G}\, \mathbf{U}$.

3.3 Time Integration — Implicit Euler

The semi-discrete system

$$\frac{d\mathbf{U}}{dt} = \mathbf{L}(\mathbf{U}) \tag{7}$$

is advanced with a fixed-step implicit (backward) Euler scheme:

$$\left(\mathbf{I} - \Delta t\, \alpha\, \mathbf{D}\, \mathbf{K}^n\, \mathbf{G}\right) \mathbf{U}^{n+1} = \mathbf{U}^n, \tag{8}$$

where $\mathbf{K}^n$ is evaluated at the current time level using $\tilde{u}_f^n$. The time step is fixed at $\Delta t = 10^{-5}$.

3.4 Boundary Condition Enforcement

Dirichlet conditions (3) are imposed via MOLE's `addScalarBC2D` utility, which modifies the system matrix and right-hand side in place before each linear solve.

3.5 Algorithm Summary

Algorithm 1 PME Solver with MOLE Mimetic Operators

Build $\mathbf{G}$, $\mathbf{D}$, $\mathbf{P}$ via `grad2D`, `div2D`, `interpol2D`
Set $\mathbf{U}^0$ from the Barenblatt profile at t_0 ▷ Eq. (4)
while $t < T$ **do**
    Interpolate cell-centered values to faces: $\tilde{\mathbf{u}}_f \leftarrow \mathbf{P}\mathbf{U}^n$
    Clip face values for coefficient assembly: $\tilde{\mathbf{u}}_f \leftarrow \max(\tilde{\mathbf{u}}_f, 0)$
    Form nonlinear diffusivity: $\mathbf{K} \leftarrow \mathrm{diag}(\tilde{\mathbf{u}}_f^m)$ ▷ Eq. (6)
    Assemble $\mathbf{M} \leftarrow \mathbf{I} - \Delta t\, \alpha\, \mathbf{DKG}$
    Set $\mathbf{b} \leftarrow \mathbf{U}^n$
    Apply Dirichlet BCs via `addScalarBC2D`$(\mathbf{M}, \mathbf{b}, \ldots)$
    Solve $\mathbf{M}\mathbf{U}^{n+1} = \mathbf{b}$
    Update $\mathbf{U}^n \leftarrow \mathbf{U}^{n+1}$
    Advance time: $t \leftarrow t + \Delta t$
end while
Compute L^2 and L^∞ errors vs. $u_{\text{exact}}(t)$ ▷ Eq. (5)

4 Numerical Results

4.1 Qualitative Comparison of Solution Profiles

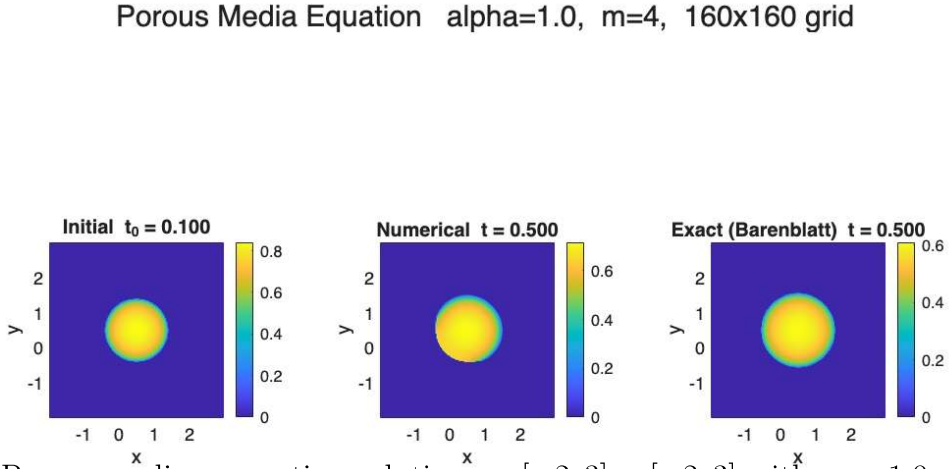

Figure 1: Porous medium equation solution on $[-2, 3] \times [-2, 3]$ with $\alpha = 1.0$, $m = 4$, and a 160×160 grid. *Left*: initial Barenblatt profile at $t_0 = 0.1$, peak value ≈ 0.9. *Centre*: numerical solution at $t = 0.5$, peak value ≈ 0.7. *Right*: exact Barenblatt solution at $t = 0.5$, peak value ≈ 0.6.

Figure 1 illustrates the evolution of the population density from $t_0 = 0.1$ to $t = 0.5$. At the initial time, the Barenblatt profile exhibits a circular compact support centered at $(0.5, 0.5)$ with a smooth, flat-topped interior characteristic of the PME with $m = 4$; the maximum density is approximately 0.9. A sharp transition to zero density at the support boundary is

clearly visible, reflecting the finite propagation speed that distinguishes the PME from linear diffusion.

By $t = 0.5$ the support has expanded radially outward, and the peak density has decreased to approximately 0.7 in the numerical solution and 0.6 in the exact Barenblatt solution. Both profiles retain the circular symmetry and flat-top shape of the self-similar solution. The numerical solution slightly overestimates the peak amplitude while reproducing the support radius and overall shape accurately. This small excess at the center is consistent with the implicit Euler scheme's tendency to introduce mild numerical diffusion, which in this context delays the decay of the peak rather than spreading the front prematurely.

The close visual agreement between the center and right panels confirms that the mimetic discretization captures the geometry of the Barenblatt solution well. Quantitative error norms are reported in Table 1.

4.2 Error Analysis

Discrete error norms are defined as

$$\|e\|_\infty = \max_{i,j} |U_{i,j}^{\text{num}} - u_{i,j}^{\text{exact}}|, \tag{9}$$

$$\|e\|_2 = \left(\Delta x \, \Delta y \sum_{i,j} |U_{i,j}^{\text{num}} - u_{i,j}^{\text{exact}}|^2 \right)^{1/2}. \tag{10}$$

Table 1: Error norms at $t = 0.5$ ($\alpha = 1$, $m = 4$, $\Delta t = 10^{-5}$, 160×160 grid).

Metric	Value
$\|e\|_2$	2.982×10^{-1}
$\|e\|_\infty$	4.395×10^{-1}
Relative L^2	3.218×10^{-1}

5 Discussion

The numerical results demonstrate that the mimetic finite-difference method implemented with MOLE captures the essential qualitative and quantitative features of the Barenblatt self-similar solution. The compact support, circular symmetry, flat-topped interior profile, and outward propagation of the front are all reproduced correctly. The L^2 error of 2.982×10^{-1} and the L^∞ error of 4.395×10^{-1} reflect the inherent difficulty of resolving the PME near the free boundary, where the solution transitions sharply from a positive value to zero. Unlike the smooth manufactured solution used in the Fisher equation report, the Barenblatt profile has a non-differentiable front, which limits the achievable accuracy of any fixed-order spatial discretization regardless of the method chosen. The largest pointwise errors are therefore concentrated at the support boundary rather than in the interior, consistent with the L^∞ error exceeding the L^2 error.

The choice of implicit Euler time integration with $\Delta t = 10^{-5}$ was motivated by the stiffness of the semi-discrete system. The linearized diffusion operator scales like h^{-2}, so an explicit scheme would require a time step $\Delta t \lesssim h^2/\max(u^m)$ for stability. With $h = 5/160 \approx 0.031$ and $m = 4$, this explicit stability limit is on the order of 10^{-3} at best, and considerably smaller near the peak where u^m is largest. The implicit Euler scheme avoids this restriction and produces stable solutions at the chosen Δt, though its first-order temporal accuracy contributes to the accumulated error over the 4000 steps from $t_0 = 0.1$ to $T = 0.5$.

The mimetic div-grad decomposition $\mathbf{D}\,\mathbf{K}\,\mathbf{G}$ mirrors the continuous structure of the PME operator exactly, ensuring that the discrete flux balance across each control volume satisfies a discrete analog of the divergence theorem. This structural consistency is particularly valuable near the domain boundary, where standard finite differences require ad hoc stencil modifications that can introduce conservation errors. The absence of spurious oscillations in the interior and the clean zero values at the walls throughout the simulation indicate that the boundary conditions were enforced correctly by `addScalarBC2D`.

Natural extensions of this work include testing higher-order MOLE operators ($k = 4$) to assess whether the improved interior accuracy reduces the free-boundary error, replacing the fixed-step implicit Euler integrator with an adaptive solver such as MATLAB's `ode15s` to better control temporal error, and exploring non-zero Dirichlet or Neumann boundary conditions to simulate population dynamics in bounded heterogeneous environments.

6 Conclusion

In this work the two-dimensional porous medium equation was solved numerically using the MOLE library's mimetic gradient and divergence operators. An implicit Euler time integration was employed to handle the stiffness introduced by the nonlinear diffusion term. The Barenblatt self-similar solution served as an exact reference for validation.

References

[1] R. Rostamian, *The Porous Medium Equation*, Chapter 21 in *A First Course in Numerical Analysis of Differential Equations*, University of Maryland, Baltimore County.

[2] J. Corbino and J. E. Castillo, High-Order Mimetic Finite-Difference Operators Satisfying the Extended Gauss Divergence Theorem, *Journal of Computational and Applied Mathematics*, 364 (2020), doi:10.1016/j.cam.2019.06.042.

[3] J. Corbino, M. Dumett, and J. E. Castillo, MOLE: Mimetic Operators Library Enhanced, *Journal of Open Source Software*, 9(99):6288, 2024. `https://doi.org/10.21105/joss.06288`

[4] J. L. Vázquez, *The Porous Medium Equation: Mathematical Theory*, Oxford University Press, 2007.